Continuous structural neuroplasticity during motor learning - a diffusion MRI study

Naama Friedman[1], Cfir Malovani[2], Inbar Perets[3], Etai Kenin[4], Michal Bernstein-Eliav[1], Ido Tavor[1,3,5]

[1]Faculty of Medicine, Tel Aviv University, Tel Aviv, Israel

[2]School of Electrical Engineering, Faculty of Engineering, Tel Aviv University, Tel Aviv, Israel

[3]Sagol School of Neuroscience, Tel Aviv University, Tel Aviv, Israel

[4]Department of Natural and Life Sciences, The Open University of Israel, Israel

[5]Strauss Center for Computational Neuroimaging, Tel Aviv University, Tel Aviv, Israel

Corresponding Author:

Dr. Ido Tavor; ORCID ID https://orcid.org/0000-0002-9117-4449

Department of Anatomy and Anthropology

Faculty of Medicine

Tel Aviv University

Ramat Aviv 6997801

Israel

idotavor@tauex.tau.ac.il

Tel: +972-73-7304420

Fax: +972-3-6408287

Abstract

Learning is a complex, continuously evolving process which induces widespread structural and functional brain alterations. In recent years, diffusion magnetic resonance imaging (dMRI) has been used to detect microstructural modifications after short learning periods. While previous studies primarily explored changes *following* learning (i.e., by comparing images acquired before and after learning), the continuous temporal dynamics of microstructural alterations *during* the encoding phase of learning itself are yet to be examined. Here, we introduce a novel approach for continuous acquisition of dMRI images which allow tracking microstructural changes throughout learning and demonstrate the utility of this approach on a motor sequence learning (finger tapping) task (n=58). Voxel-wise analysis revealed a decrease in mean diffusivity (MD) in task-related brain regions, including the parahippocampal gyrus, hippocampus, inferior temporal gyrus, and cerebellum. Further analysis of the temporal patterns of decrease revealed a rapid MD reduction in the right temporal gyrus after 11 minutes of learning, with additional decrease in the right parahippocampal gyrus and left cerebellum after 22 minutes. We computed "neuroplasticity networks" of brain areas showing similar change patterns and detected similarities between these networks and canonical functional connectivity networks. Our findings offer novel insights on the spatio-temporal dynamics of neuroplasticity and advance our understanding of motor learning by demonstrating continuous microstructural modifications from the very first minutes of training.

Keywords

Neuroplasticity; Learning; Diffusion MRI; Motor sequence learning; DTI; Finger tapping

1. Introduction

Learning takes time. It requires an intricate, multi-staged process in both space and time, such that different brain regions are involved in encoding, consolidation, and retention of the newly acquired skill (Dahms et al., 2020). While the development of new skills can occur over extended periods of practice and experience (Green and Bavelier, 2008; Knight et al., 2017), learning-related neural modifications are evident already at the very first minutes of encoding (Brodt et al., 2018; Sagi et al., 2012; Tavor et al., 2020). To fully understand the neural underpinnings of learning it is crucial to consider its continuously evolving nature.

Numerous studies have explored the structural and functional alterations that accompany learning using structural and functional magnetic resonance imaging (MRI), respectively. Over the last decade, diffusion-weighted MRI (dMRI) has also been employed to study short-term microstructural neuroplasticity (Brodt et al., 2018; Hofstetter et al., 2017; Jacobacci et al., 2020; Keller and Just, 2016; Sagi et al., 2012; Tavor et al., 2020, 2013; Villemonteix et al., 2023). dMRI measures the translational displacement of water molecules (Bihan and Warach, 1995) and is mainly used for white matter assessment and reconstruction (Catani et al., 2002; Moseley et al., 1990; Warach et al., 1992). By scanning the displacement of water molecules across various spatial orientations, a mathematical representation, the diffusion tensor, can be constructed (Basser et al., 1994). From that tensor, it is possible to calculate quantitative information about the tissue microstructure as summation indices, such as the mean diffusivity (MD) and the fractional anisotropy (FA), as well as define the prime directions of water diffusion.

The MD is a scalar representation of the diffusion tensor, reflecting the amount of diffusivity in the tissue. It depends on the composition of the tissue and on its

components - making it sensitive to the tissue's microstructure. The calculation of the MD is orientation-invariant; it is, therefore, comparable across subjects and scans (Assemlal et al., 2011). In several studies, a learning-induced decrease in MD was found after training in multiple cognitive domains, such as motor, spatial, lingual, and others (Hofstetter et al., 2017; Sagi et al., 2012; Sampaio-Baptista et al., 2013; Taubert et al., 2010; Tavor et al., 2020, 2013). The biological substrates underlying the reduction in MD may include changes in the extracellular matrix (Van Der Toorn et al., 1996), formation of synapses and dendrites (Toni et al., 1999), dendritic remodelling, axonal sprouting and pruning (Kays et al., 2012), neurogenesis (Knoth et al., 2010; Maćkowiak et al., 2002; Seib and Martin-Villalba, 2015), astrocyte remodelling (Assaf, 2018; Blumenfeld-Katzir et al., 2011; Sagi et al., 2012) or other modifications in several types of glial cells (Fields et al., 2014; Weston et al., 2015). MD may be therefore used as an anatomical biomarker for neuroplasticity.

Previous neuroplasticity studies have focused on different timeframes of brain changes, ranging from a few months to just a few days (Thomas and Baker, 2013), and on different cognitive domains such as spatial navigation (Keller and Just, 2016; Sagi et al., 2012; Tavor et al., 2013; Villemonteix et al., 2023), motor sequence training (Jacobacci et al., 2020; Tavor et al., 2020), language (Hofstetter et al., 2017) and associative memory (Brodt et al., 2018). Notably, these studies have investigated the differences in brain microstructure between two discrete timepoints: before and after a learning routine. However, the temporal dynamics of the learning process itself, and what transpires within the brain during that time, have not been fully explored yet. This study aims to monitor the continuous microstructural changes occurring in the brain during the learning process itself. To achieve this, we employed a unique dMRI protocol that enables the continuous acquisition of diffusion images throughout task

performance. We computed a continuous MD measurement and used it to identify temporal patterns of neuroplasticity across the brain, to detect the exact changepoint in MD during learning and to define 'neuroplasticity networks' of brain regions that share common microstructural modification patterns.

2. Methods

2.1 Participants

Sixty-two right-handed healthy volunteers with no history of neurological disease, psychiatric disorders, drug or alcohol abuse, or use of neuropsychiatric medication were recruited. Four participants were excluded due to technical issues during the scan or excessive movement, resulting in a final sample of fifty-eight participants (30 females, mean age = 27.66, SD = 4.4). Participants were randomly assigned to either a learning group (14 females, mean age = 28.47, SD = 4.26) or a control group (16 females, mean age = 26.5, SD = 4.37). The experimental protocol was approved by the Institutional Review Board of the Sheba Medical Center and all participants signed an informed consent form.

2.2 Experimental procedure

Participants underwent an MRI session which included a dMRI scan and several structural scans. During the dMRI scan, participants in the learning group performed a motor sequence learning task (see details below) while participants in the control group were instructed to focus on a fixation cross and not perform any explicit task. MRI acquisition was carried out in The Alfredo Federico Strauss Center for Computational Neuroimaging at Tel Aviv University.

2.3 MRI acquisition

Scans were acquired on a 3T whole-body MRI system (Siemens Magnetom Prisma) equipped with a 64-channel head coil.

Diffusion-weighted images (DWI) were acquired with a spin-echo diffusion-weighted, echo-planar imaging sequences with up to 68 axial slices (whole-brain coverage) and a resolution of 2×2×2 mm^3, with a TR/TE = 3,500/59.4ms, multiband acceleration factor = 2. Diffusion parameters were: Δ/δ= 28/10ms, b-value of 1,000s/mm^2 were taken at 589 gradient directions with additional 33 non-diffusion weighted (b_0) images (spread evenly across the scan duration to serve as a reference to assess diffusion-related decay of the MR signal for each tensor calculation). The total dMRI scan duration was 36:28 minutes. In addition, five b_0 images and one b_{1000} image were acquired with a reversed phase-encoding direction to correct for susceptibility-induced distortions.

T1 weighted images were acquired with a magnetization prepared rapid gradient echo (MPRAGE) sequence with up to 176 axial slices (whole-brain coverage), TR/TE = 2,400/2.98ms, resolution of 0.9×0.9×0.9 mm^3, scan time of 4:30 minutes. T2-weighted images were acquired with up to 176 slices (whole-brain coverage), TR/TE = 3,200/554, resolution of 0.9×0.9×0.9 mm^3, scan time of 5 minutes. In addition, FLAIR images (TR/TE/TI = 8,000/81/2,370) were acquired for radiological screening.

2.4 Motor sequence learning task

Participants in the learning group performed a finger tapping task (first introduced by Karni et al., 1995). The task consisted of 24 trials of 60 seconds, each followed by a 25-second rest period, for a total duration of 33:35 minutes, with additional 2:53 minutes of rest at the end of the task. During task trials, participants were instructed

to repeat a 5-digit sequence (2-4-1-3-2) using their left (non-dominant) hand as correctly and quickly as possible, while the sequence is constantly presented on the screen to eliminate executive memory differences. Rest periods were added to allow for offline gain learning (Bönstrup et al., 2019; Jacobacci et al., 2020). Finally, participants performed an additional task trial while in the scanner, but with no scan being performed, serving as a behavioral test.

2.5 Behavioral assessment

Two measurements of task performance were calculated: (1) accuracy: the total amount of correct sequences completed, calculated as the number of correct sequences a participant performed within a specific trial, and (2) speed: the mean duration of a successful key press sequence, calculated as the average duration of correct sequences in a specific trial (sequence duration being the time passed between pressing the first and last keys of a sequence). Both measurements were computed for each trial and for the test trial. Paired t-tests were performed for each of these measurements, between the first and last trials, and the test trial.

2.6 dMRI data analysis

dMRI images were corrected for head motion, susceptibility-induced distortions, and eddy currents-induced distortions, as well as registered to the T1w image using the minimal preprocessing pipeline proposed by the Human connectome project (Glasser et al., 2013; Sotiropoulos et al., 2013) including FSL's TOPUP and EDDY tools (Andersson et al., 2003; Andersson and Sotiropoulos, 2016). For optimized registration to the MNI space we applied a tissue-probability based registration routine, as recently described by Malovani et al., 2021. Data was spatially smoothed with a FWHM of 5 mm using FSL.

To obtain a continuous measurement of microstructural changes during learning, we calculated the diffusion tensor by applying a sliding window approach: We used a window length of 13 TRs (12 DWI images plus one non-diffusion weighted (b_0) image), and a window offset of a single TR. To determine the window length, we used data from ten HCP participants (Van Essen et al., 2012) who underwent a dMRI scan containing 90 different gradient directions at b=1000 s/mm^2. We calculated the MD from an increasing number of directions, ranging from 6 to 87 (to allow for an adequate number of possible permutations, or $\max_k \binom{90}{k} > 10^4$). To calculate stability, we created 1000 permutations for each number of directions, and calculated MD each time using a different set of directions. Stability was defined by the standard deviation (SD) of the average MD in gray matter and white matter for each number of gradient directions (Supplementary Figure S1A). The stability of the MD measurement increased with the number of directions used, with more than 11 directions resulting in near-zero values of SD across permutations (Supplementary Figure S1B). Therefore, we concluded that 12 gradient directions are sufficient for a stable MD calculation. Window offset was set to 1 TR to maximize the number of MD timepoints. Considering these window length and offsets, and a TR of 3.5 seconds, an MD timepoint was calculated based on 42 seconds of data and the difference between MD timepoints was 3.5 seconds. MD values were calculated along the timeseries of the DWI scan, resulting in a continuous measurement of MD during learning (Figure 1). All analyses were performed in MATLAB (2020b, Natick, Massachusetts: The MathWorks Inc).

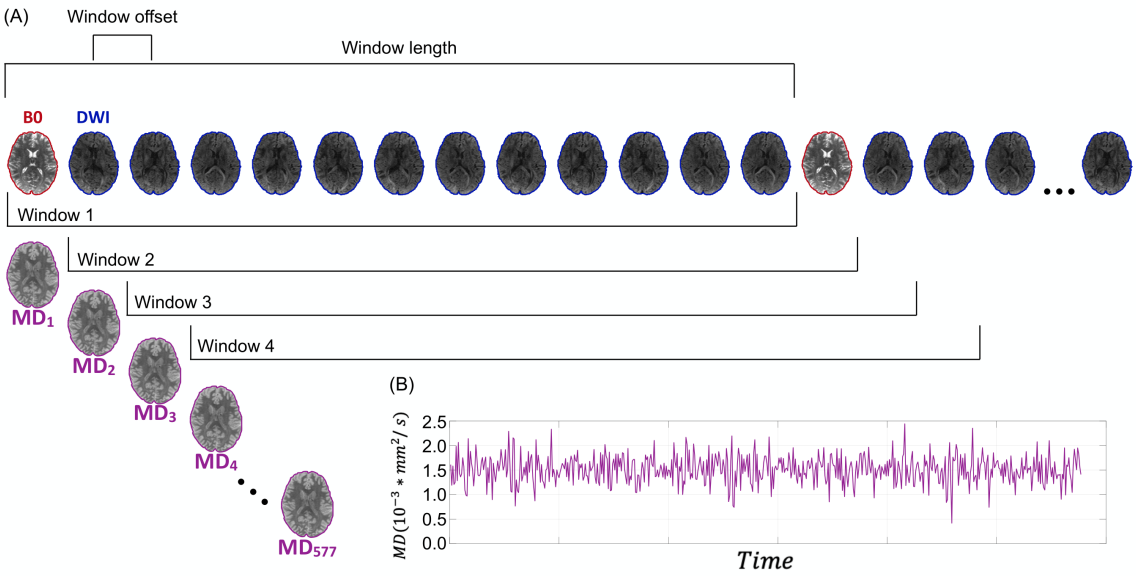

Figure 1. Continuous MD using a sliding window approach. (A) An illustration of a sliding window over multiple diffusion weighted images (DWI) volumes. Window length was set to 13 TRs (12 DWI images in different gradient directions + one b_0 volume) and the window offset was one TR. **(B)** For each window, an MD value in each voxel was calculated to create a continuous measurement of microstructural properties.

In addition to this continuous characterization of MD changes, we also calculated MD "pre" and "post" learning, as the mean MD in the first and last ten MD timepoints in the continuous MD curve, respectively (see Supplementary Figure S2 for the same analysis with 1, 5 or 15 MD timepoints).

To further explore the evolving pattern of MD changes during learning, we investigated discrete timepoints along the continuous MD curve shown in Figure 1B. Specifically, we computed the percent change in MD between the "pre learning" timepoint (as described above) and three additional timepoints: around 11 minutes into the learning process, around 22 minutes into the learning process, and at the end of the scan, after learning is completed, which is identical to the "pre"/"post" comparison described above. Each of these additional points was calculated as the mean of 10 MD timepoints, starting at 11 or 22 minutes into learning. Since an MD timepoint lasted 42 seconds and was separated by 3.5 seconds from the next one, 10 MD timepoints

lasted $42 + (3.5 * 9) = 73.5$ seconds (i.e., “11 minutes into learning” was the mean MD from the 11th minute to the 12 minute and 13.5 seconds, and “22 minutes into learning” was the mean MD from the 22nd minute to 23 and 13.5 seconds).

2.7 Statistical analysis

To detect clusters of MD decrease, that were later used for investigation of continuous modifications during the learning process itself, we first performed a voxel-wise two-way ANOVA of MD timepoint (before / after learning) X Group (learning/control) using FSL’s PALM tool with 1000 permutations (Winkler et al., 2014). Only gray matter voxels were included, and a threshold-free cluster enhancement (Smith and Nichols, 2009) was utilized. P-values were FDR corrected for multiple comparisons. Clusters with over 50 voxels that showed an interaction effect (i.e., MD decrease in the learning but not the control group) were included in following stages of analysis.

For each of these clusters, we computed the “pre” and “post” learning MD as described above, as well as the differences between the “pre-learning” MD and the additional timepoints throughout the learning process, averaged within the learning or control groups. Paired t-tests were performed between the “pre-learning” MD and the three subsequent timepoints (11 minutes, 22 minutes, and post-learning).

Next, to obtain a continuous characterization of MD change, we averaged MD values per MD timepoint within each cluster across voxels and across participants for each group independently and received two distinct MD timeseries per cluster (for the learning and control groups). To visually display the MD change patterns, we smoothed the time series using a 100-point moving average.

To further compare between the patterns of MD change across clusters, we performed a changepoint analysis (Killick et al., 2012) per smoothed timeseries to detect the

timepoint in which the greatest change in slope has occurred for each cluster. To achieve a more detailed understanding of the spatial pattern of temporal changes, changepoint analysis was additionally used to examine the change in slope separately for each voxel within a cluster.

We next examined the similarities between microstructural plasticity patterns across brain areas. This analysis was performed for the learning group only. Gray matter was parcelled into 300 cortical areas (Schaefer et al., 2018) and additional 64 sub-cortical areas (Brainnetomme atlas; Fan et al., 2016). For each region, we computed the average continuous MD change across voxels and participants. We then computed Pearson's correlations between all region pairs. We applied a hierarchical clustering using Python library SciPy (Virtanen et al., 2020) to detect "neuroplasticity networks", i.e., networks of brain areas that share similar temporal patterns of MD change during learning. This analysis resulted in a division of the brain into five "networks" (the number of clusters was determined by finding the optimal division based on the average within-cluster distance (Supplementary Figure S3)). To examine the correspondence between these "neuroplasticity networks" and known functional networks, we computed the Dice index between each of the main four "neuroplasticity networks" (excluding the smallest) and the seven canonical resting-state functional connectivity networks (Yeo et al., 2011). For the same analysis with an alternative parcellation, using the Brainnetome atlas (BNA) only, see Supplementary Figures S4-S6.

3. Results

3.1 Behavioural results

Participants showed successful learning in both accuracy and speed (Figure 2). Comparing the first and last trials of learning, the mean improvement in speed was 42.9% (SE = 2.8%) and the mean improvement in accuracy was 67.2% (SE = 11.2%). In the test trial, performed after a 12-minute break (inside the scanner), the improvement in speed was 52.3% (SE = 2.2%) and in accuracy, 108.55% (SE =14.7%) compared to the first trial. Differences between the first, last and test trials were significant for both measurements (paired t-test, p < 0.001, FDR corrected).

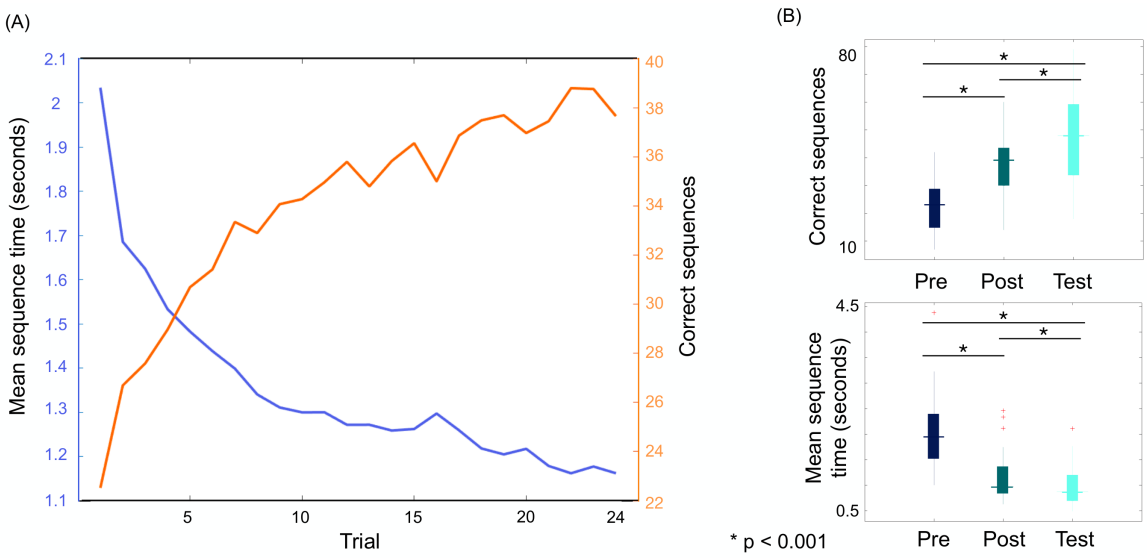

Figure 2. **Behavioral effects of motor sequence learning. (A)** Averaged behavioral scores for 29 participants who performed a finger tapping task for 33:35 minutes (24 trials). The figure shows, on the right y axis, the mean sequence duration per trial, and on the left y axis the mean number of correct sequences per trial. **(B)** Differences in performance between the first, last and test trials (paired t-test, $p < 0.001$, FDR corrected).

3.2 Microstructural neuroplasticity at discrete timepoints throughout learning

In a voxel-wise two-way ANOVA of MD timepoint (before/after learning) X group (learning/control) we found a 1-4% MD decrease in the right parahippocampal gyrus (PHG), the right hippocampus, the right inferior temporal gyrus (ITG) and the cerebellum (Figure 3A and B). To further explore the evolving pattern of MD decrease

during learning, we examined additional timepoints throughout the learning process. Each panel in Figure 3C includes, therefore, three bars, depicting MD change between the “pre-learning” baseline and the following timepoints: around 11 minutes into the learning process; around 22 minutes into the learning process; and after learning is completed, which is identical to the bars shown in Figure 3B. A rapid reduction in MD within the right temporal gyrus was observed after 11 minutes of learning, extending consistently until task's completion. A decrease in MD was also observed after 22 minutes of learning in the right PHG and the left cerebellum.

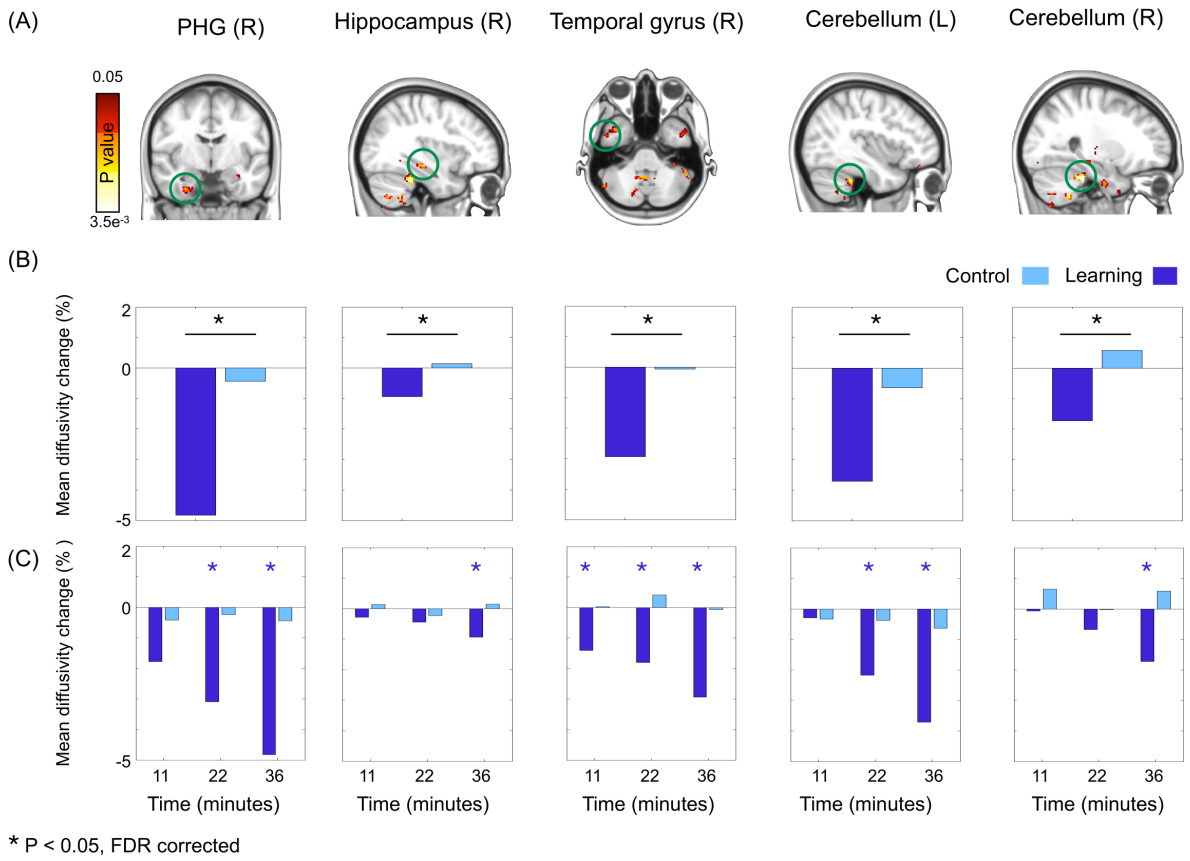

Figure 3. **Microstructural neuroplasticity at discrete timepoints throughout motor sequence learning. (A)** We first examined the pre/post learning effect following training: A 2 (learning vs. control groups) by 2 (pre/post) ANOVA revealed a significant interaction effect. Clusters of MD decrease following learning were found in the right parahippocampal gyrus (PHG), the right hippocampus, the right inferior temporal gyrus, and the cerebellum. **(B)** MD change in the clusters displayed in A, for the learning (dark blue) and control groups (light blue). **(C)** A three-point temporal course of MD change in the same clusters. Paired t-tests were performed between each timepoint and the pre-learning timepoint, asterisks denote a significant MD decrease in the learning group.

3.3 Continuous training-induced neuroplasticity

The continuous MD change during learning is presented in Figure 4. Notably, within all clusters, the reduction in MD manifested gradually during learning; however, distinct variations were detected across regions.

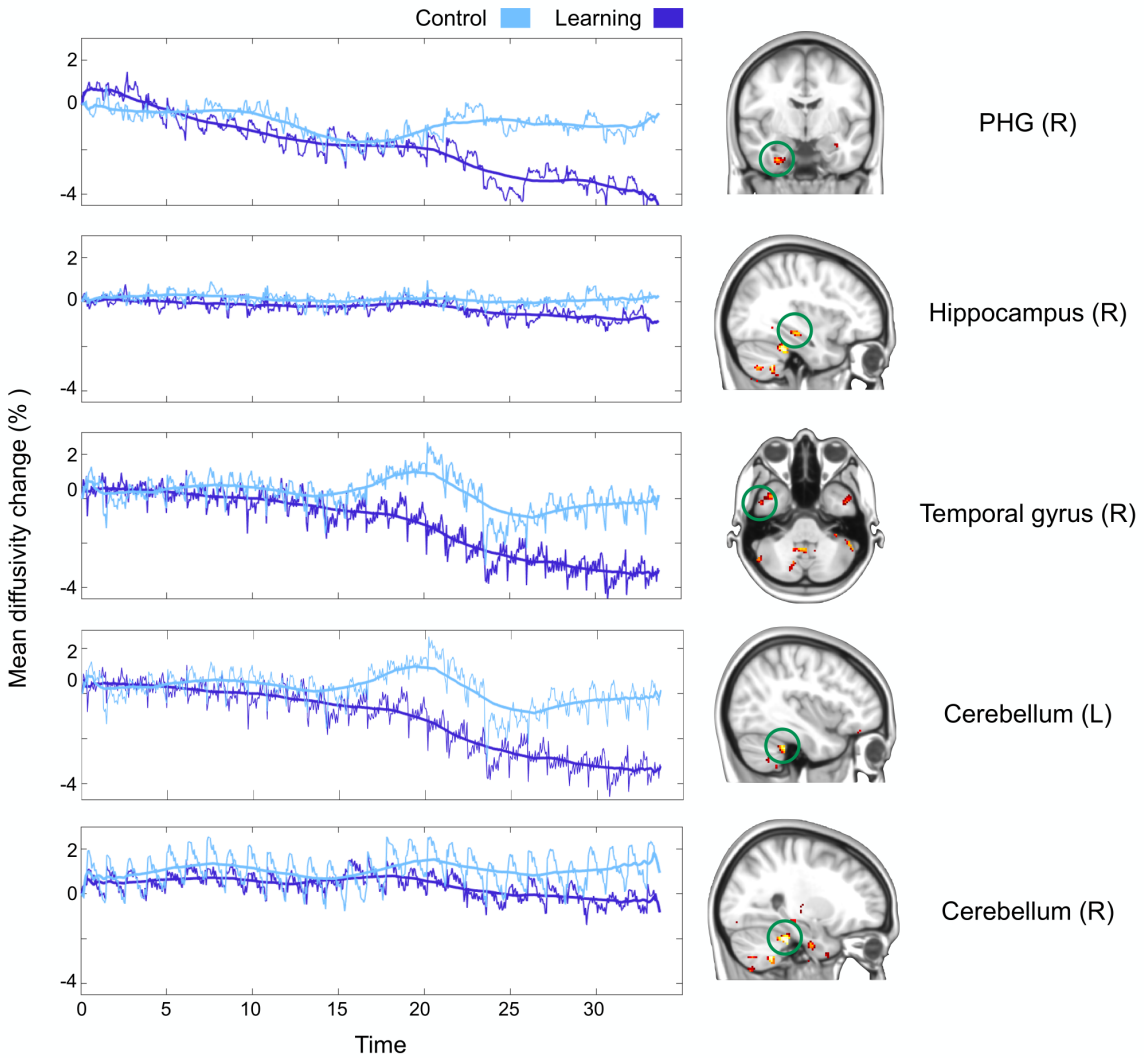

Figure 4. **Continuous MD changes during learning.** While a decrease in MD was found in all areas for the learning group compared to the control group, the patterns of decrease differed across areas. A 100-points smoothed curve is displayed to represent the trend of MD reduction during learning, averaged within group.

In Figure 5, we present the results of a changepoint analysis aimed to examine variations in the slope of MD decrease across clusters. Notably, in the parahippocampal gyrus we observed a relatively consistent slope throughout the learning process, while in the hippocampus and cerebellum we detected a significant

changepoint occurring approximately 15 minutes into the learning task. During subsequent phases of learning, the MD decrease was considerably steeper compared to initial stages (Figure 5A).

It is worth highlighting that variations in the progression of MD decrease were not only evident between different brain regions but also within each area. For instance, in the cerebellum, we identified voxels displaying a change in slope around the 15-minute mark, while others exhibit this change at later timepoints (Figure 5B, see Supplementary Figure S7 for the voxelwise changepoint analysis results in other clusters).

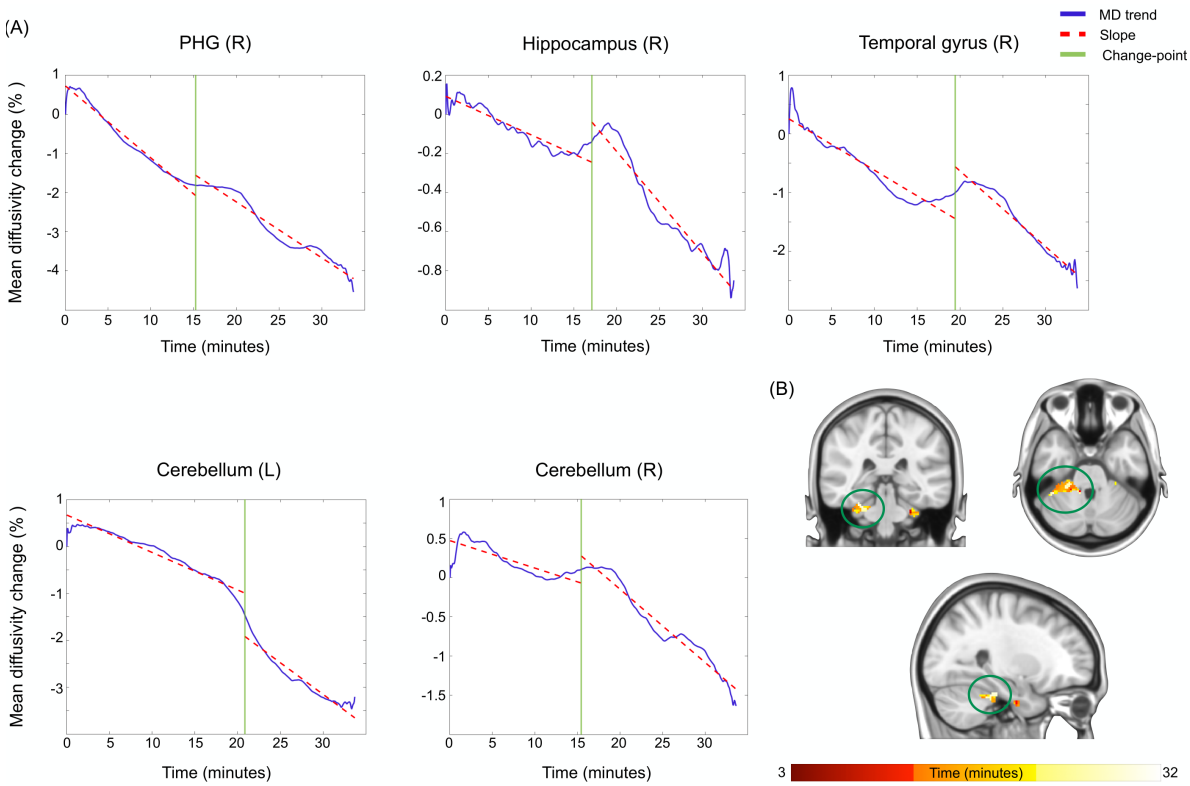

Figure 5. **Changepoint detection analysis. (A)** For each of the five clusters, a change in slope was determined as the maximum change between the slope of the two parts of the divided curve. **(B)** Voxelwise changepoint detection within the cerebellum. Color-coding represents the time (minutes into the learning process) of changepoint for each voxel in the right cerebellum.

3.4 Neuroplasticity networks

We next searched for "neuroplasticity networks", reflecting a network-level organization of brain regions that undergo similar microstructural changes during learning. To examine the similarities in the patterns of MD decrease across brain regions, we first parcelled the brain into 364 areas based on the Schaefer parcellation of 300 cortical areas and the BNA atlas for 64 subcortical areas. We then calculated the continuous MD for each parcel across all participants and computed the Pearson's correlations between each pair of parcels, resulting in a 364x364 correlation matrix. Based on hierarchical clustering (with the number of clusters determined by finding the optimal division based on the average within-cluster distance (Supplementary Figure S3)), we characterized four "plasticity networks" (Figure 6).

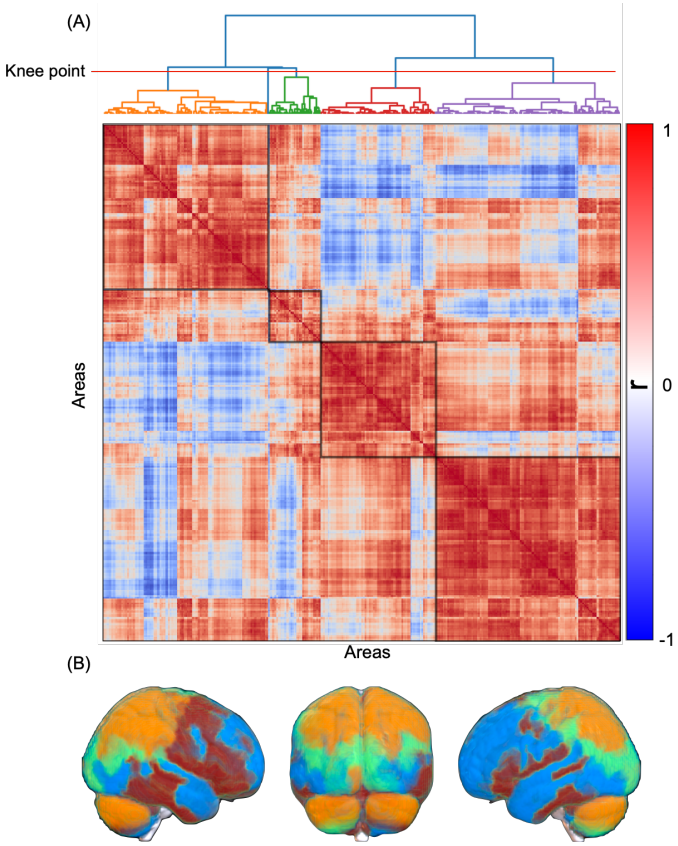

Figure 6. **Neuroplasticity networks. (A)** A matrix depicting the pairwise Pearson's correlations between the patterns of MD decrease across 364 brain regions, ordered by a hierarchical clustering algorithm and parcelled to "plasticity networks" (black squares). **(B)** The four main networks displayed on an inflated surface of the brain.

Finally, we examined the correspondence between these networks and canonical functional connectivity networks (Yeo et al., 2011) by computing the Dice index between each pair of networks (Figure 7). Similarities were detected between each of our “neuroplasticity networks” and either the somatomotor, the default mode or the visual networks.

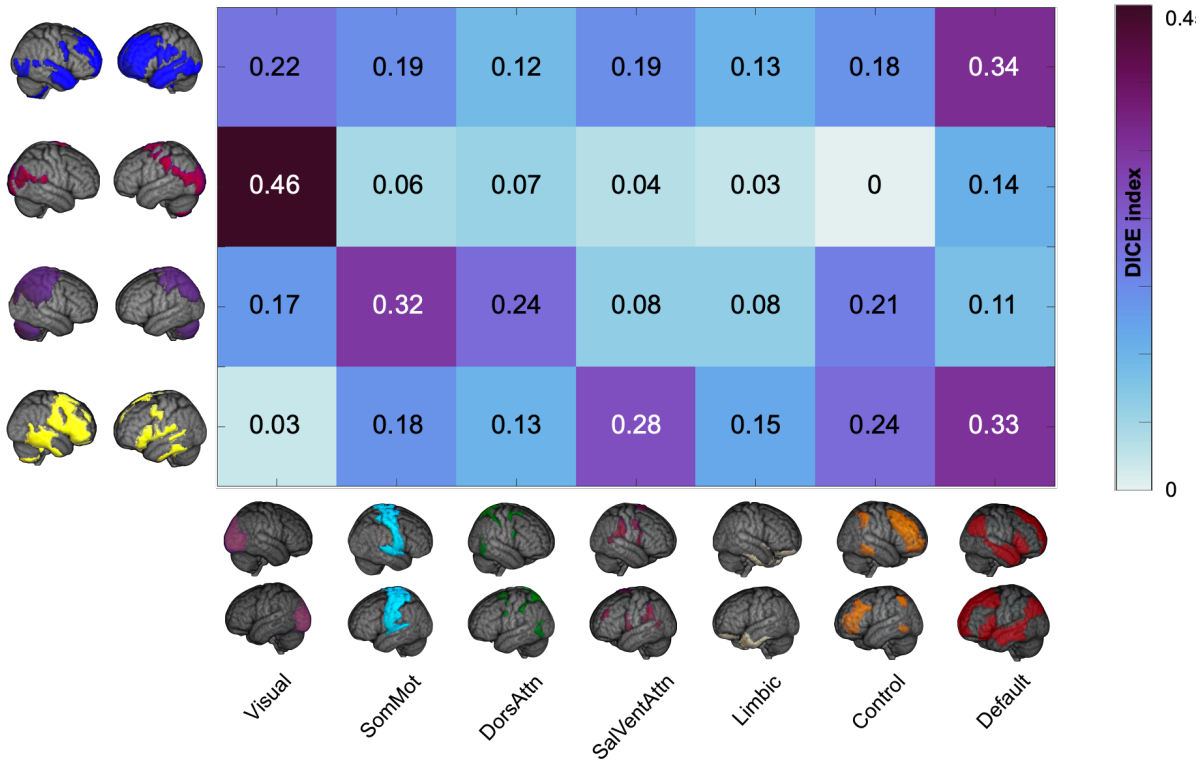

Figure 7. **Similarities between neuroplasticity networks and functional connectivity networks.** Similarity matrix showing the Dice index between each of our four main neuroplasticity networks and Yeo’s seven connectivity networks. Highest Dice indices were found between the neuroplasticity networks and the somatomotor network (Dice = 0.32), the default network (Dice = 0.34) and the visual network (Dice = 0.46).

4. Discussion

In this work we investigate continuous learning-induced microstructural remodelling of brain tissue, leveraging a unique diffusion MRI protocol to continuously assess mean diffusivity (MD) throughout a motor learning routine. Different patterns of MD decrease were found in several learning-related brain areas, suggesting an involvement of these areas at the different stages of learning. Specifically, while the parahippocampal gyrus demonstrated a relatively consistent slope of MD decrease, the hippocampus and cerebellum showed a significant change in slope 15 to 20 minutes into the learning process. Furthermore, we were able to capture different change patterns across single voxels within a cluster, suggesting high sensitivity of our method to the spatio-temporal properties of learning-induced changes. Finally, based on similarities in the patterns of MD decrease across the brain we detected “neuroplasticity networks”, consisting of areas that undergo similar microstructural alterations during learning.

Our main goal was to examine where do signatures of neuroplasticity develop in the brain and how they change over ongoing training. While the use of diffusion MRI to study short-term microstructural plasticity has gained increasing interest over the last decade (Brodt et al., 2018; Hofstetter et al., 2017; Jacobacci et al., 2020; Keller and Just, 2016; Sagi et al., 2012; Tavor et al., 2020, 2013; Villemonteix et al., 2023), these studies have all investigated the differences in brain structure between two discrete timepoints: before and after learning. This work is therefore the first to explore the temporal dynamics of microstructural changes as they occur during the encoding stage of the learning process itself.

Motor sequence learning requires a complex ensemble of distributed brain regions which are involved at different stages of learning (Dahms et al., 2020; Penhune and

Steele, 2012; Tavor et al., 2020). For example, a twenty-year-old influential model has suggested that early stages of learning involve cortico-cerebellar and cortico-striatal mechanisms, whereas later stages of consolidation and retention engage the striatum, motor and parietal cortices (Doyon et al., 2003). The emergence of a long-term memory representation of the newly learned skill has been suggested to involve a gradual transition from a rich and unique representation in the hippocampus to a more abstract, generalized version in the neocortex (Brodt et al., 2016; Moscovitch et al., 2016; Sekeres et al., 2018). Our results go beyond these classical models of learning by 'zooming in' into the very first minutes of motor learning, tracking continuous changes and detecting the exact moments in time when different brain areas join the process.

Of particular interest is the involvement of the hippocampus, which challenges traditional theories of a slow transfer from the hippocampus to the neocortex (Moscovitch et al., 2016; Sekeres et al., 2018) but is in line with more recent work, showing an early engagement of the hippocampus during learning (Brodt et al., 2018; Jacobacci et al., 2020). Our findings support a role of the hippocampus in short-term memory stabilization (Schapiro et al., 2019) or in connecting encoded items of different modalities over space or time (Buzsáki and Tingley, 2018). The hippocampus may reactivate information about the learned motor sequence, similar to memory replay described in rodents (Foster, 2017), which may explain microstructural remodelling of the hippocampus 15 minutes into the learning process.

While it is evident that the unique diffusion MRI protocol developed here is sensitive to dynamic, flexible brain modifications over short timescales, the biological underpinnings of such modifications are yet to be fully understood. A possible explanation is that learning-induced alterations in MD may reflect the rapid

modification of astrocytes structures during and following learning (Assaf, 2018; Johansen-Berg et al., 2012; Sagi et al., 2012; Tavor et al., 2013).

The division to ‘neuroplasticity networks’ based on similarities of MD change patterns across brain regions offers further insights into the complex, multi-regional process that ultimately gives rise to learning and memory. These networks are not to be confused with the widely studied functional or structural networks, which reflect the temporal synchronization in brain activity across regions or the physical connections between them, respectively. Considering the accumulating evidence on a high correspondence between functional connectivity and brain activity (Gal et al., 2022; Smith et al., 2009; Tavor et al., 2016; Tik et al., 2023, 2021) and the recent suggestion that functional network architecture may relate brain activity and behaviour (Bernstein-Eliav and Tavor, 2022; Bijsterbosch et al., 2020), a network-organization approach may facilitate the study of neuroplasticity and its behavioural manifestation as well. Specifically, grouping areas by the patterns of microstructural changes may shed new light on the intricate mechanisms underlying skill acquisition.

An examination of the hierarchical clustering results reveals that the largest ‘neuroplasticity networks’ may roughly correspond with the functionally-defined somatomotor and default mode networks (Yeo et al., 2011), which is consistent with the known involvement of frontal, temporal and parietal cortices in motor sequence learning (Turesky et al., 2018; Witt et al., 2008). This correspondence is particularly intriguing as Yeo’s networks are defined based on the functional MRI signal during resting-state while our ‘neuroplasticity networks’ are driven from diffusion properties during task performance. It may therefore provide converging evidence for neuroplasticity mechanisms supported by brain areas within the somatomotor network, including the primary motor and surrounding cortices which play a critical role

in motor learning and execution, and the default mode network, including associative cortices in the frontal and parietal lobes that are thought to be involved in memory retrieval and self-referential processing (Raichle, 2015). Interestingly, disrupted functional connections between these networks have also been associated with motor dysfunction in neurodegenerative disorders (Chenji et al., 2016).

This work introduces a novel method to continuously track diffusion properties throughout learning. Our results provide a promising proof-of-concept, yet further research is required to examine methodological aspects and optimize parameters such as window length and offset. It should also be considered that due to the nature of MD, which is calculated based on a series of DWI images acquired from various directions at intervals of a few seconds (depending on the repetition time, TR), the temporal resolution of our method is lower than that of functional imaging methods such as fMRI or even functional diffusion MRI (fdMRI) (Le Bihan, 2003; Nunes et al., 2021, 2019; Tsurugizawa et al., 2013). Therefore, further research is required to address the correspondence between these different imaging methods and integrate between them to achieve a more comprehensive picture on the temporal dynamics of learning-induced changes. Additionally, in this study we employed a relatively simple motor learning task; future work may apply our method to study higher-level cognitive tasks and complex learning routines. Insights on the timing and the network-level organization of learning-induced microstructural changes may extend previous findings on neuroplasticity following spatial navigation (Keller and Just, 2016; Sagi et al., 2012; Tavor et al., 2013; Villemonteix et al., 2023), language (Hofstetter et al., 2017) and associative memory tasks (Brodt et al., 2018).

To conclude, we provide evidence for the utility of a continuous acquisition of diffusion MRI during task performance to explore the dynamic aspects of microstructural

neuroplasticity. Rather than a single, post-learning 'snapshot' that indicates that changes have occurred at some, undetectable, point and pace, we show that different task-related brain areas demonstrate distinctive temporal patterns of learning-related modifications. The continuous characterization of neuroplasticity is therefore a promising approach, offering a temporally sensitive, network-level view on the orchestrated processes underlying learning and memory in the human brain.

5. Data and Code Availability

The code used for continuous MD calculation is available at: https://github.com/naamaf/Continuous_DTI. Raw MRI data cannot be shared due to data protection, but we provide tables of continuous MD values across parcels in the code repository.

6. Author Contributions

Naama Friedman: Conceptualization, Data collection and Curation, Methodology, Writing - Original Draft; Cfir Malovani: Formal analysis, Validation; Inbar Paretz: Data collection; Etai Kenin: Data collection; Michal Bernstein-Eliav: Writing – Review & Editing; Ido Tavor: Supervision, Conceptualization, Writing - Review & Editing.

7. Funding

Funding for this research was provided by the Minducate Science of Learning Research and Innovation Center of the Sagol School of Neuroscience, Tel Aviv University, and the Israeli Science Foundation (ISF Grant no. 1603/18).

8. Declaration of Competing Interests

The authors have no conflict of interests to disclose.

9. Acknowledgements (optional)

Data used for method optimization were provided by the Human Connectome Project, WU-Minn Consortium (Principal Investigators: David Van Essen and Kamil Ugurbil; 1U54MH091657) funded by the 16 NIH Institutes and Centers that support the NIH Blueprint for Neuroscience Research; and by the McDonnell Center for Systems Neuroscience at Washington University.

10. References

1. Andersson, J.L.R., Skare, S., Ashburner, J., 2003. How to correct susceptibility distortions in spin-echo echo-planar images: Application to diffusion tensor imaging. Neuroimage 20, 870–888. https://doi.org/10.1016/S1053-8119(03)00336-7
2. Andersson, J.L.R., Sotiropoulos, S.N., 2016. An integrated approach to correction for off-resonance effects and subject movement in diffusion MR imaging. Neuroimage 125, 1063–1078. https://doi.org/10.1016/j.neuroimage.2015.10.019
3. Assaf, Y., 2018. New dimensions for brain mapping. Science (1979) 362, 994–995. https://doi.org/10.1126/science.aav7357
4. Assemlal, H.E., Tschumperlé, D., Brun, L., Siddiqi, K., 2011. Recent advances in diffusion MRI modeling: Angular and radial reconstruction. Med Image Anal 15, 369–396. https://doi.org/10.1016/j.media.2011.02.002
5. Basser, P.J., Mattiello, J., LeBihan, D., 1994. MR diffusion tensor spectroscopy and imaging. Biophys J 66, 259–267. https://doi.org/10.1016/S0006-3495(94)80775-1
6. Bernstein-Eliav, M., Tavor, I., 2022. The Prediction of Brain Activity from Connectivity: Advances and Applications. Neuroscientist 10738584221130974. https://doi.org/10.1177/10738584221130974
7. Bihan, D. Le, Warach, S.J., 1995. Diffusion and perfusion magnetic resonance imaging: applications to functional MRI. J Comput Assist Tomogr 844.
8. Bijsterbosch, J., Harrison, S.J., Jbabdi, S., Woolrich, M., Beckmann, C., Smith, S., Duff, E.P., 2020. Challenges and future directions for representations of functional brain organization. Nat Neurosci 23, 1484–1495. https://doi.org/10.1038/s41593-020-00726-z
9. Blumenfeld-Katzir, T., Pasternak, O., Dagan, M., Assaf, Y., 2011. Diffusion MRI of Structural Brain Plasticity Induced by a Learning and Memory Task. PLoS One 6, e20678. https://doi.org/10.1371/journal.pone.0020678
10. Bönstrup, M., Iturrate, I., Thompson, R., Cruciani, G., Censor, N., Cohen, L.G., 2019. A Rapid Form of Offline Consolidation in Skill Learning. Current Biology 29, 1346-1351.e4. https://doi.org/10.1016/J.CUB.2019.02.049
11. Brodt, S., Gais, S., Beck, J., Erb, M., Scheffler, K., Schönauer, M., 2018. Fast track to the neocortex: A memory engram in the posterior parietal cortex. Science (1979) 362, 1045–1048. https://doi.org/10.1126/science.aau2528
12. Brodt, S., Pöhlchen, D., Flanagin, V.L., Glasauer, S., Gais, S., Schönauer, M., 2016. Rapid and independent memory formation in the parietal cortex. Proc Natl Acad Sci U S A 113, 13251–13256. https://doi.org/10.1073/pnas.1605719113
13. Buzsáki, G., Tingley, D., 2018. Space and Time: The Hippocampus as a Sequence Generator. Trends Cogn Sci 22, 853–869. https://doi.org/10.1016/j.tics.2018.07.006

14. Catani, M., Howard, R.J., Pajevic, S., Jones, D.K., 2002. Virtual in Vivo Interactive Dissection of White Matter Fasciculi in the Human Brain. Neuroimage 17, 77–94. https://doi.org/10.1006/NIMG.2002.1136
15. Chenji, S., Jha, S., Lee, D., Brown, M., Seres, P., Mah, D., Kalra, S., 2016. Investigating default mode and sensorimotor network connectivity in amyotrophic lateral sclerosis. PLoS One 11, 1–14. https://doi.org/10.1371/journal.pone.0157443
16. Dahms, C., Brodoehl, S., Witte, O.W., Klingner, C.M., 2020. The importance of different learning stages for motor sequence learning after stroke. Hum Brain Mapp 41, 270–286. https://doi.org/10.1002/hbm.24793
17. Doyon, J., Penhune, V., Ungerleider, L.G., 2003. Distinct contribution of the cortico-striatal and cortico-cerebellar systems to motor skill learning. Neuropsychologia 41, 252–262. https://doi.org/10.1016/S0028-3932(02)00158-6
18. Fan, L., Li, H., Zhuo, J., Zhang, Y., Wang, J., Chen, L., Yang, Z., Chu, C., Xie, S., Laird, A.R., Fox, P.T., Eickhoff, S.B., Yu, C., Jiang, T., 2016. The Human Brainnetome Atlas: A New Brain Atlas Based on Connectional Architecture. Cerebral Cortex 26, 3508–3526. https://doi.org/10.1093/cercor/bhw157
19. Fields, R.D., Araque, A., Johansen-Berg, H., Lim, S.S., Lynch, G., Nave, K.A., Nedergaard, M., Perez, R., Sejnowski, T., Wake, H., 2014. Glial biology in learning and cognition. Neuroscientist 20, 426–431. https://doi.org/10.1177/1073858413504465
20. Foster, D.J., 2017. Replay Comes of Age. Annu Rev Neurosci 40, 581–602. https://doi.org/10.1146/annurev-neuro-072116-031538
21. Gal, S., Tik, N., Bernstein-Eliav, M., Tavor, I., 2022. Predicting individual traits from unperformed tasks. Neuroimage 249, 118920. https://doi.org/10.1016/j.neuroimage.2022.118920
22. Glasser, M.F., Sotiropoulos, S.N., Wilson, J.A., Coalson, T.S., Fischl, B., Andersson, J.L., Xu, J., Jbabdi, S., Webster, M., Polimeni, J.R., Van Essen, D.C., Jenkinson, M., 2013. The minimal preprocessing pipelines for the Human Connectome Project. Neuroimage 80, 105–124. https://doi.org/10.1016/j.neuroimage.2013.04.127
23. Green, C.S., Bavelier, D., 2008. Exercising Your Brain: A Review of Human Brain Plasticity and Training-Induced Learning. Psychol Aging 23, 692–701. https://doi.org/10.1037/a0014345
24. Hofstetter, S., Friedmann, N., Assaf, Y., 2017. Rapid language-related plasticity: microstructural changes in the cortex after a short session of new word learning. Brain Struct Funct 222, 1231–1241. https://doi.org/10.1007/s00429-016-1273-2
25. Jacobacci, F., Armony, J.L., Yeffal, A., Lerner, G., Amaro, E., Jovicich, J., Doyone, J., Della-Maggiore, V., 2020. Rapid hippocampal plasticity supports motor sequence

learning. Proc Natl Acad Sci U S A 117, 23898–23903. https://doi.org/10.1073/pnas.2009576117

26. Johansen-Berg, H., Baptista, C.S., Thomas, A.G., 2012. Human Structural Plasticity at Record Speed. Neuron 73, 1058–1060. https://doi.org/10.1016/j.neuron.2012.03.001
27. Karni, A., Meyer, G., Jezzard, P., Adams, M.M., Turner, R., Ungerleider, L.G., Kami, A., Meyer, G., Jezzard, P., Adams, M.M., Turner, R., Ungerleider, L.G., 1995. Functional MRI evidence for adult motor cortex plasticity during motor skill learning. Nature 1995 377:6545 377, 155–158. https://doi.org/10.1038/377155a0
28. Kays, J.L., Hurley, R.A., Taber, K.H., 2012. The dynamic brain: Neuroplasticity and mental health. Journal of Neuropsychiatry and Clinical Neurosciences 24, 118–124. https://doi.org/10.1176/appi.neuropsych.12050109
29. Keller, T.A., Just, M.A., 2016. Structural and functional neuroplasticity in human learning of spatial routes. Neuroimage 125, 256–266. https://doi.org/10.1016/j.neuroimage.2015.10.015
30. Killick, R., Fearnhead, P., Eckley, I.A., 2012. Optimal detection of changepoints with a linear computational cost. J Am Stat Assoc 107, 1590–1598. https://doi.org/10.1080/01621459.2012.737745
31. Knight, S., Friend Wise, A., Chen, B., 2017. Time for Change: Why Learning Analytics Needs Temporal Analysis. Journal of Learning Analytics 4. https://doi.org/10.18608/jla.2017.43.2
32. Knoth, R., Singec, I., Ditter, M., Pantazis, G., Capetian, P., Meyer, R.P., Horvat, V., Volk, B., Kempermann, G., 2010. Murine Features of Neurogenesis in the Human Hippocampus across the Lifespan from 0 to 100 Years. PLoS One 5, e8809. https://doi.org/10.1371/journal.pone.0008809
33. Le Bihan, D., 2003. Looking into the functional architecture of the brain with diffusion MRI. Nat Rev Neurosci 4, 469–480. https://doi.org/10.1038/nrn1119
34. Maćkowiak, M., Chocyk, A., Markowicz-Kula, K., Wedzony, K., Gage, F.H., Fred H. Gage, 2002. Neurogenesis in the adult brain. Pol J Pharmacol. https://doi.org/10.1523/jneurosci.22-03-00612.2002
35. Malovani, C., Friedman, N., Ben-Eliezer, N., Tavor, I., 2021. Tissue Probability Based Registration of Diffusion-Weighted Magnetic Resonance Imaging. Journal of Magnetic Resonance Imaging 54, 1066–1076. https://doi.org/10.1002/jmri.27654
36. Moscovitch, M., Cabeza, R., Winocur, G., Nadel, L., 2016. Episodic Memory and Beyond: The Hippocampus and Neocortex in Transformation. Annu Rev Psychol 67, 105–34. https://doi.org/10.1146/annurev-psych-113011-143733
37. Moseley, M.E., Cohen, Y., Kucharczyk, J., Mintorovitch, J., Asgari, H.S., Wendland, M.F., Tsuruda, J., Norman, D., 1990. Diffusion-weighted MR imaging of anisotropic

water diffusion in cat central nervous system. https://doi.org/10.1148/radiology.176.2.2367658 176, 439–445. https://doi.org/10.1148/RADIOLOGY.176.2.2367658

38. Nunes, D., Gil, R., Shemesh, N., 2021. A rapid-onset diffusion functional MRI signal reflects neuromorphological coupling dynamics. Neuroimage 231, 117862. https://doi.org/10.1016/j.neuroimage.2021.117862
39. Nunes, D., Ianus, A., Shemesh, N., 2019. Layer-specific connectivity revealed by diffusion-weighted functional MRI in the rat thalamocortical pathway. Neuroimage 184, 646–657. https://doi.org/10.1016/j.neuroimage.2018.09.050
40. Penhune, V.B., Steele, C.J., 2012. Parallel contributions of cerebellar, striatal and M1 mechanisms to motor sequence learning. Behavioural Brain Research 226, 579–591. https://doi.org/10.1016/j.bbr.2011.09.044
41. Raichle, M.E., 2015. The Brain's Default Mode Network. Annu Rev Neurosci 38, 433–447. https://doi.org/10.1146/annurev-neuro-071013-014030
42. Sagi, Y., Tavor, I., Hofstetter, S., Tzur-Moryosef, S., Blumenfeld-Katzir, T., Assaf, Y., 2012. Learning in the fast lane: new insights into neuroplasticity. Neuron 73, 1195–203. https://doi.org/10.1016/j.neuron.2012.01.025
43. Sampaio-Baptista, C., Khrapitchev, A.A., Foxley, S., Schlagheck, T., Scholz, J., Jbabdi, S., DeLuca, G.C., Miller, K.L., Taylor, A., Thomas, N., Kleim, J., Sibson, N.R., Bannerman, D., Johansen-Berg, H., 2013. Motor skill learning induces changes in white matter microstructure and myelination. J Neurosci 33, 19499–503. https://doi.org/10.1523/JNEUROSCI.3048-13.2013
44. Schaefer, A., Kong, R., Gordon, E.M., Laumann, T.O., Zuo, X.-N., Holmes, A.J., Eickhoff, S.B., Yeo, B.T.T., 2018. Local-Global Parcellation of the Human Cerebral Cortex from Intrinsic Functional Connectivity MRI. Cerebral Cortex 28, 3095–3114. https://doi.org/10.1093/cercor/bhx179
45. Schapiro, A.C., Reid, A.G., Morgan, A., Manoach, D.S., Verfaellie, M., Stickgold, R., 2019. The hippocampus is necessary for the consolidation of a task that does not require the hippocampus for initial learning. Hippocampus 29, 1091–1100. https://doi.org/10.1002/hipo.23101
46. Seib, D.R.M., Martin-Villalba, A., 2015. Neurogenesis in the Normal Ageing Hippocampus: A Mini-Review. Gerontology 61, 327–335. https://doi.org/10.1159/000368575
47. Sekeres, M.J., Winocur, | Gordon, Moscovitch, M., Anderson, J.A.E., Pishdadian, S., Wojtowicz, | J Martin, St-Laurent, M., Mcandrews, M.P., Grady, C.L., 2018. Changes in patterns of neural activity underlie a time-dependent transformation of memory in rats and humans. Hippocampus 28, 745–764. https://doi.org/10.1002/hipo.23009

48. Smith, S.M., Fox, P.T., Miller, K.L., Glahn, D.C., Fox, P.M., Mackay, C.E., Filippini, N., Watkins, K.E., Toro, R., Laird, A.R., Beckmann, C.F., 2009. Correspondence of the brain's functional architecture during activation and rest. Proc Natl Acad Sci U S A 106, 13040–13045. https://doi.org/10.1073/pnas.0905267106
49. Smith, S.M., Nichols, T.E., 2009. Threshold-free cluster enhancement: Addressing problems of smoothing, threshold dependence and localisation in cluster inference. Neuroimage 44, 83–98. https://doi.org/10.1016/j.neuroimage.2008.03.061
50. Sotiropoulos, S.N., Jbabdi, S., Xu, J., Andersson, J.L., Moeller, S., Auerbach, E.J., Glasser, M.F., Hernandez, M., Sapiro, G., Jenkinson, M., Feinberg, D.A., Yacoub, E., Lenglet, C., Van Essen, D.C., Ugurbil, K., Behrens, T.E.J., 2013. Advances in diffusion MRI acquisition and processing in the Human Connectome Project. Neuroimage 80, 125–143. https://doi.org/10.1016/j.neuroimage.2013.05.057
51. Taubert, M., Draganski, B., Anwander, A., Müller, K., Horstmann, A., Villringer, A., Ragert, P., 2010. Dynamic properties of human brain structure: Learning-related changes in cortical areas and associated fiber connections. Journal of Neuroscience 30, 11670–11677. https://doi.org/10.1523/JNEUROSCI.2567-10.2010
52. Tavor, I., Botvinik-Nezer, R., Bernstein-Eliav, M., Tsarfaty, G., Assaf, Y., 2020. Short-term plasticity following motor sequence learning revealed by diffusion magnetic resonance imaging. Hum Brain Mapp 41, 442–452. https://doi.org/10.1002/hbm.24814
53. Tavor, I., Hofstetter, S., Assaf, Y., 2013. Micro-structural assessment of short term plasticity dynamics. Neuroimage 81, 1–7. https://doi.org/10.1016/j.neuroimage.2013.05.050
54. Tavor, I., Parker Jones, O., Mars, R.B., Smith, S.M., Behrens, T.E., Jbabdi, S., 2016. Task-free MRI predicts individual differences in brain activity during task performance. Science 352, 216–20. https://doi.org/10.1126/science.aad8127
55. Thomas, C., Baker, C.I., 2013. Teaching an adult brain new tricks: A critical review of evidence for training-dependent structural plasticity in humans. Neuroimage. https://doi.org/10.1016/j.neuroimage.2012.03.069
56. Tik, N., Gal, S., Madar, A., Ben-David, T., Bernstein-Eliav, M., Tavor, I., 2023. Generalizing prediction of task-evoked brain activity across datasets and populations. Neuroimage 276, 120213. https://doi.org/10.1016/j.neuroimage.2023.120213
57. Tik, N., Livny, A., Gal, S., Gigi, K., Tsarfaty, G., Weiser, | Mark, Tavor, I., 2021. Predicting individual variability in task-evoked brain activity in schizophrenia. Hum Brain Mapp 42, 3983–3992. https://doi.org/10.1002/hbm.25534
58. Toni, N., Buchs, P.A., Nikonenko, I., Bron, C.R., Muller, D., 1999. LTP promotes formation of multiple spine synapses between a single axon terminal and a dendrite. Nature 402, 421–425. https://doi.org/10.1038/46574

59. Tsurugizawa, T., Ciobanu, L., Le Bihan, D., 2013. Water diffusion in brain cortex closely tracks underlying neuronal activity. Proc Natl Acad Sci U S A 110, 11636–11641. https://doi.org/10.1073/pnas.1303178110
60. Turesky, T.K., Olulade, O.A., Luetje, M.M., Eden, G.F., 2018. An fMRI study of finger tapping in children and adults. Hum Brain Mapp 39, 3203–3215. https://doi.org/10.1002/hbm.24070
61. Van Der Toorn, A., Syková, E., Dijkhuizen, R.M., Voříšek, I., Vargová, L., Škobisová, E., Van Lookeren Campagne, M., Reese, T., Nicolay, K., 1996. Dynamic changes in water ADC, energy metabolism, extracellular space volume, and tortuosity in neonatal rat brain during global ischemia. Magn Reson Med 36, 52–60. https://doi.org/10.1002/MRM.1910360110
62. Van Essen, D.C., Ugurbil, K., Auerbach, E., Barch, D., Behrens, T.E.J., Bucholz, R., Chang, A., Chen, L., Corbetta, M., Curtiss, S.W., Della Penna, S., Feinberg, D., Glasser, M.F., Harel, N., Heath, A.C., Larson-Prior, L., Marcus, D., Michalareas, G., Moeller, S., Oostenveld, R., Petersen, S.E., Prior, F., Schlaggar, B.L., Smith, S.M., Snyder, A.Z., Xu, J., Yacoub, E., 2012. The Human Connectome Project: A data acquisition perspective. Neuroimage. https://doi.org/10.1016/j.neuroimage.2012.02.018
63. Villemonteix, T., Guerreri, M., Deantoni, M., Balteau, E., Schmidt, C., Stee, W., Zhang, H., Peigneux, P., 2023. Sleep-dependent structural neuroplasticity after a spatial navigation task: A diffusion imaging study. J Neurosci Res 101, 1031–1043. https://doi.org/10.1002/jnr.25176
64. Virtanen, P., Gommers, R., Oliphant, T.E., Haberland, M., Reddy, T., Cournapeau, D., Burovski, E., Peterson, P., Weckesser, W., Bright, J., van der Walt, S.J., Brett, M., Wilson, J., Millman, K.J., Mayorov, N., Nelson, A.R.J., Jones, E., Kern, R., Larson, E., Carey, C.J., Polat, İ., Feng, Y., Moore, E.W., VanderPlas, J., Laxalde, D., Perktold, J., Cimrman, R., Henriksen, I., Quintero, E.A., Harris, C.R., Archibald, A.M., Ribeiro, A.H., Pedregosa, F., van Mulbregt, P., Vijaykumar, A., Bardelli, A. Pietro, Rothberg, A., Hilboll, A., Kloeckner, A., Scopatz, A., Lee, A., Rokem, A., Woods, C.N., Fulton, C., Masson, C., Häggström, C., Fitzgerald, C., Nicholson, D.A., Hagen, D.R., Pasechnik, D. V., Olivetti, E., Martin, E., Wieser, E., Silva, F., Lenders, F., Wilhelm, F., Young, G., Price, G.A., Ingold, G.L., Allen, G.E., Lee, G.R., Audren, H., Probst, I., Dietrich, J.P., Silterra, J., Webber, J.T., Slavič, J., Nothman, J., Buchner, J., Kulick, J., Schönberger, J.L., de Miranda Cardoso, J.V., Reimer, J., Harrington, J., Rodríguez, J.L.C., Nunez-Iglesias, J., Kuczynski, J., Tritz, K., Thoma, M., Newville, M., Kümmerer, M., Bolingbroke, M., Tartre, M., Pak, M., Smith, N.J., Nowaczyk, N., Shebanov, N., Pavlyk, O., Brodtkorb, P.A., Lee, P., McGibbon, R.T., Feldbauer, R., Lewis, S., Tygier, S., Sievert, S., Vigna, S., Peterson, S., More, S., Pudlik, T., Oshima, T., Pingel, T.J.,

Robitaille, T.P., Spura, T., Jones, T.R., Cera, T., Leslie, T., Zito, T., Krauss, T., Upadhyay, U., Halchenko, Y.O., Vázquez-Baeza, Y., 2020. SciPy 1.0: fundamental algorithms for scientific computing in Python. Nat Methods 17, 261–272. https://doi.org/10.1038/s41592-019-0686-2

65. Warach, S., Chien, D., Li, W., Ronthal, M., Edelman, R.R., 1992. Fast magnetic resonance diffusion-weighted imaging of acute human stroke. Neurology 42, 1717–1717. https://doi.org/10.1212/WNL.42.9.1717
66. Weston, P.S.J., Simpson, I.J.A., Ryan, N.S., Ourselin, S., Fox, N.C., 2015. Diffusion imaging changes in grey matter in Alzheimer's disease: A potential marker of early neurodegeneration. Alzheimers Res Ther 7, 1–8. https://doi.org/10.1186/s13195-015-0132-3
67. Winkler, A.M., Ridgway, G.R., Webster, M.A., Smith, S.M., Nichols, T.E., 2014. Permutation inference for the general linear model. Neuroimage 92, 381–397. https://doi.org/10.1016/j.neuroimage.2014.01.060
68. Witt, S.T., Laird, A.R., Meyerand, M.E., 2008. Functional neuroimaging correlates of finger-tapping task variations: An ALE meta-analysis. Neuroimage 42, 343–356. https://doi.org/10.1016/j.neuroimage.2008.04.025
69. Yeo, B.T., Krienen, F.M., Sepulcre, J., Sabuncu, M.R., Lashkari, D., Hollinshead, M., Roffman, J.L., Smoller, J.W., Zöllei, L., Polimeni, J.R., Fisch, B., Liu, H., Buckner, R.L., 2011. The organization of the human cerebral cortex estimated by intrinsic functional connectivity. J Neurophysiol 106, 1125–1165. https://doi.org/10.1152/jn.00338.2011